

Chemical characterization of organic compounds involved in iodine-initiated new particle formation from coastal macro-algal emission

Yibei Wan¹, Xiangpeng Huang², Chong Xing¹, Qiongqiong Wang¹, Xinlei Ge², Huan Yu^{1,*}

¹ School of Environmental Studies, China University of Geosciences, Wuhan, 430074, China

² Jiangsu Key Laboratory of Atmospheric Environment Monitoring and Pollution Control, Collaborative Innovation Center of Atmospheric Environment and Equipment Technology, School of Environmental Science and Engineering, Nanjing University of Information Science and Technology, Nanjing 210044, China

* To whom correspondence should be addressed: yuhuan@cug.edu.cn

Abstract

Iodine-initiated new particle formation (I-NPF) has long been recognized in coastal hotspot regions. However, no prior work has studied the exact chemical composition of organic compounds and their role in the coastal I-NPF. Here we present an important complementary study to the ongoing laboratory and field researches of iodine nucleation in coastal atmosphere. Oxidation and NPF experiments with vapor emissions from real-world coastal macroalgae were simulated in a bag reactor. On the basis of comprehensive mass spectrometry measurements, we reported for the first time a variety of volatile precursors and their oxidation products in gas and particle phases in such a highly complex system. Organic compounds overwhelmingly dominated over iodine in the new particle growth initiated by iodine species. The identity and transformation mechanisms of organic compounds were proposed in this study to provide a more complete story of coastal NPF from low-tide macroalgal emission.

1. Introduction

Coastal new particle formation (NPF) may be driven by daytime low-tide emission of iodine species from macroalgae fully or partially exposed to the air. The phenomenon was reported in hotspot locations of west Europe, Australia and polar regions (O'dowd et al., 2002; Heard et al., 2006; Mcfiggans et al., 2010; Whitehead et al., 2009; Sipil et al., 2016; Allan et al., 2015; Baccarini et al., 2020; Beck et al., 2021). In the southeast coastline of China, we reported intense iodine-initiated NPF based on particle number size distribution and iodine measurements (Yu et al., 2019).

To simulate iodine-initiated NPF (I-NPF) in controlled laboratory conditions, I_2 or CH_2I_2 vapor was usually photolyzed in the presence of ozone to provide nucleation precursors (Burkholder et al., 2004; Jimenez et al., 2003; Monahan et al., 2012; Saunders and Plane, 2005; O'dowd et al., 2004; Gómez Mart í et al., 2020; He et al., 2021; Huang et al., 2022; Gómez Mart í et al., 2022). Ashu-Ayem et al. (2012); Monahan et al. (2012); Mcfiggans et al. (2004); Sellegri et al. (2005) and Sellegri et al. (2016) also investigated the NPF from the vapors emitted by real-world macroalgal specimens or seawater in laboratory chamber or apparatus. However, the focus of all above studies are emission rate, oxidation mechanisms or nucleation pathways of iodine species. For example, positive correlations between particle concentrations and I_2 or CH_2I_2 mixing ratios were usually observed (Burkholder et al., 2004; Jimenez et al., 2003; Sellegri et al., 2005; Monahan et al., 2012). Kinetic studies in flow tube or CERN CLOUD chamber proposed the clustering of iodine oxides (I_xO_y) or iodine oxoacids (HIO_3 , HIO_2) as nucleation mechanisms on the basis of photoionization TOF-MS (Gómez Mart í et al., 2020), Api-TOF and nitrate-Chemical Ionization Mass Spectrometer (CIMS) measurements (He et al., 2021; Gómez Mart í et al., 2022).

Organic compounds have also been suggested to be involved in coastal NPF (Vaattovaara et al., 2006; Yu et al., 2019). Huang et al. (2022) and Saunders et al. (2010) investigated the effect of uptake of meso-erythritol, glyoxal, dimethylamine and oxalic acid on the growth of iodine oxide nanoparticles. However, no prior work has investigated the exact chemical identity of organic compounds (other than iodomethane) and their role in I-NPF. The role of biogenic terpenes and anthropogenic aromatics in continental NPF has been recognized for a long time (Donahue et al., 2013). Their ozonolysis or photochemistry products have been investigated in depth by using Electrospray Ionization Mass Spectrometry (ESI-MS) and more recently, CIMS (Nguyen et al., 2010; Kundu et al., 2017; Kundu et al., 2012; Faxon et al., 2018; Wang et al., 2020; Riva et al., 2017; Yan et al., 2020; Ehn et al., 2014). It is very likely that certain volatile organic compounds (VOCs) emitted mutually with iodine or iodinated methane from coastal biota or biologically active sea surface may also be involved in coastal I-NPF process and promote the growth of iodine particles.

To test this hypothesis, we conducted oxidation and NPF experiments with vapor emissions from real-world coastal macroalgae in a bag reactor. A suite of mass spectrometric methods including Inductively Coupled Plasma-MS (ICP-MS), Gas Chromatography-MS (GC-MS), iodide-CIMS and ESI-orbitrap MS were applied to measure vapor precursors, gaseous products and particulate products during the NPF process. Mass concentrations of total organic carbon (TOC) and total iodine (TI) of new particles were compared to evaluate the relative importance of organics and iodine in new particle growth. The identity and transformation mechanisms of organic compounds were

65 identified to provide a more complete story of coastal NPF from low-tide macroalgal emission. Our
66 study is thus complementary to prior laboratory and field studies of I-NPF, but has an emphasis on
67 organics.

68 2. Experiments

69 2.1 Experimental apparatus and sample collection

70 Similar to Potential Aerosol Mass (PAM) Oxidation Flow Reactor, a bag reactor was designed to
71 provide an oxidizing environment for simulating atmospheric oxidation processes of algae-emitted
72 VOCs. The bag reactor was made from 75 μm -thick fluorinated ethylene propylene (FEP) Teflon
73 (1.2 m \times 1.5 m, flat dimension). The volume of the bag at full inflation was determined
74 experimentally to be about 200 L. The bag was suspended vertically (Figure 1) and kept in the dark
75 or directly exposed to room light of fluorescent lamp. Before each experiment, the bag was purged
76 for several hours to reduce background particle concentrations to below 1 cm^{-3} .

77 *Undaria pinnatifida*, a common brown seaweed species at Xiangshan gulf of east China coast,
78 was collected from local intertidal zone and stored at -10 $^{\circ}\text{C}$ until the experiments. 2 kg macroalgae
79 was put in a 20 L Pyrex glass bottle that was filled with \sim 1 L natural seawater. The specimens was
80 partially exposed to the air to simulate tidal emersion of macroalgae. A flow of particle-free ultra
81 high purity (UHP) air blew algae-emitted VOCs out of the bottle and merged with a diluting air flow
82 before entering the bag reactor.

83 Two types of experiments were conducted. In the three ozonolysis experiments, ozone (O_3) was
84 generated by flowing an UHP air flow through a 5 Watt 185 nm UV lamp. The O_3 flow was fed just
85 before the bag reactor was fully inflated. Final O_3 concentration in the bag reactor was measured to
86 be \sim 500 ppbv using an ozone analyzer (Model 49i, Thermo-Fisher Scientific Inc.). RH was estimated
87 to be 10% in the bag reactor assuming 0.3 lpm water-saturated VOC flow was diluted by 2.7 lpm dry
88 air flow. In an additional OH-enhanced experiment, the O_3 /VOC mixture flow was directed through a
89 254 nm UV light before entering the bag reactor. OH radicals were produced via the reaction
90 $\text{O}_3+h\nu\rightarrow\text{O}_2+\text{O}(^1\text{D})$ and $\text{O}(^1\text{D})+\text{H}_2\text{O}\rightarrow 2\text{OH}$. Integrated OH exposure time was determined by SO_2
91 decay experiment to be 2.4 days in the experimental apparatus assuming ambient average OH
92 concentration 1.5×10^6 molecules cm^{-3} (see Supporting Material S1). Other oxidants may include
93 $\text{O}(^3\text{P})$ resulted from the quenching of $\text{O}(^1\text{D})$ (Li et al., 2015). Because the purpose of this study is to
94 identify gas and particle products of algae-emitted VOCs in the simulated NPF event, significantly
95 higher oxidation level in the bag reactor than atmosphere should not change the conclusions in the

article. Wall loss, aerosol yield, reaction rate and other kinetic factors in the bag reactor were also not evaluated.

The bag reactor was first operated in a static mode to monitor the time evolution of gaseous products and particle size. In the static mode, the bag was first filled to full inflation with the VOCs/O₃ flows. The flows were then shut down; a Scanning Mobility Particle Sizer (SMPS, model 3936, TSI Inc., Shoreview, MN, USA) and an Aerodyne iodide-CIMS pulled two flows of 0.3 liters per minute (lpm) and 1.8 lpm out of the bag, respectively. The SMPS measured the particle number size distribution from 14 to 600 nm.

The bag reactor was then operated in a dynamic mode for a few hours to collect enough particles for offline chemical analysis. In the dynamic mode, the VOCs/O₃ flow of 3 lpm was fed to the bag continuously, while the SMPS and a vacuum pump (GAST Group Ltd.) pulled sample flows of 0.3 and 2.7 lpm, respectively, out of the bag reactor. This resulted in an overall residence time of 67 minutes for the O₃/VOC mixture in the fully inflated bag. The particles in the 2.7 lpm sample flow were collected onto a Zefluer® PTFE membrane filter mounted in a filter inlet for gases and aerosols (FIGAERO) for iodide-CIMS analysis, or alternatively, onto 47 mm diameter double quartz fiber filter pack mounted in a filter holder for ESI-orbitrap MS, ICP-MS and TOC analysis. The front filter of the double filter pack collected the particles and also adsorbed some volatile species as positive artifact, while the back filter placed downstream of the front filter was supposed to adsorb the same amount of volatile species as the front filter.

2.2 Chemical analysis

Before the ozonolysis experiments, the algae-emitted VOCs in the bag reactor were collected by a 6-liter pre-evacuated stainless-steel canisters (Entech Instruments, Inc., Simi Valley, CA, USA) and analyzed using a quadrupole GC-MS system (model TH-300B, Wuhan Tianhong Instruments Co. Ltd., Wuhan, China). The algae-emitted VOCs, as well as their gaseous and particulate products, were also measured by the FIGAERO-iodide-CIMS. Iodide-adduct chemical ionization is well suited for measuring oxygenated or acidic compounds with minimal fragmentation. More details of the GC-MS and FIGAERO-iodide-CIMS measurements can be found in Supporting Material S2. The theory and design of the two instruments were described by Wang et al. (2014) and Lopez-Hilfiker et al. (2014).

The particles collected on quartz fiber filters were sent for offline quantification of TOC and TI, as well as non-target analysis of organic compounds using ESI-orbitrap MS. The front and back

filters were treated, separately, following the procedure as below: the filter was ultrasonicated twice with 10-mL water and acetone nitrile solvent mixture (v:v=1:1). Ultrasonication time and power were 20 minutes and 150 Watt. The extract was filtered by a 0.2 μ m PTFE syringe filter and evaporated in a rotary evaporator to 0.5 mL. After being centrifuged for 30 min at 12000 rpm, the supernatant was collected for TI analysis by Agilent 1100 HPLC-7900 ICP-MS (Agilent Technologies, Santa Clara, CA, USA) and TOC analysis by a TOC analyzer (Model TOC-5000A, Shimadzu, Japan). TI or TOC in the particles was obtained by subtracting the amount on the back filter from that on the front filter. Nontarget analysis of organic compounds in the supernatant was conducted using a Q Exactive hybrid Quadrupole-Orbitrap mass spectrometer (Thermo Scientific, Bremen, Germany). The supernatant was directly infused by a syringe pump and ionized in negative ESI source. All the ions in the m/z range from 50 to 500 Th were scanned with a mass resolution of 70000. The chemically sound CHO molecular formulas were computed with a mass tolerance of ± 2 ppm for these ions. Only the compounds that existed solely in the front filter or with ion intensity in the front filter higher than that in the back filter by a factor of 3 were regarded as the organic compounds in the particle phase (Wang et al., 2017).

3. Results and discussion

No particles formed in the absence of room light or O₃. Therefore, light was on throughout the experiments reported in the article. In the static mode experiments, we could not observe gas-phase products until 48 minutes after O₃ injection. New particles larger than 14 nm were observed only 58 minutes after O₃ injection. Afterwards, new particles begun to grow to form a typical banana-shape particle size spectrum (Figure 2a). This relatively long waiting time was likely due to the build-up of O₃ and oxidation products. Time zero of Figure 2 was thus set as the time when gaseous products first appeared.

3.1 Macroalgal emission

It is of particular interest to know what VOCs are emitted from coastal macroalgae. They are potential precursors of iodine particle nucleation and growth. The canister sampling followed by GC-MS analysis showed that the top 9 non-CHO compounds with highest TIC peak areas (Table 1) are C₅ alkanes, C₁₀ alpha-pinene and halogenated C₁, C₃ and C₅ alkanes. The top 10 CHO compounds are C₂-C₆ alcohols and carbonyls with saturated or unsaturated carbon chain.

Iodide-CIMS is more sensitive to more oxygenated or acidic compounds and thus complementary to the GC-MS measurement. The 76 organic precursors detected by iodide-CIMS before ozone

addition were characterized by $C_{1,2,3,6}$ and O_{2-3} formulas (Figure 3a). The top 7 compounds with highest ion intensities were CH_2O_2 , $C_2H_4O_2$, $C_3H_6O_3$, $C_6H_{10}O_3$, $C_2H_6O_2$, $C_4H_8O_2$ and $C_6H_{12}O_3$, which accounted for 82.5% of total ion intensity. They are C_1 - C_6 mono-carboxylic acids, hydroxyl carboxylic acids or oxo-carboxylic acids with 2 to 3 oxygen atoms (Table 1). Their carbon atom numbers are in general consistent with the VOCs detected by GC-MS.

Relatively high signals of NO_3^- and HNO_3I^- were observed before the addition of ozone to the bag reactor. They were likely HNO_3 or nitrate vaporized from algal specimens or natural seawater. Because NO_3^- and HNO_3I^- were also observed in the particle phase during the NPF (Figure 4), we assume HNO_3 was also an important precursor of particle formation.

3.2 Gaseous products

3.2.1 Gaseous inorganic molecules and radicals

Being different from nitrate-CIMS, our iodide-CIMS did not detect nucleating clusters of iodine oxides or oxyacids after the addition of ozone. Instead, dozens of new inorganic molecules or radicals were observed as clusters with I^- , NO_3^- or deprotonated ions in the gas or particle phase (Figure 4). We grouped these species by elemental composition and investigated their role in the NPF by observing how their gaseous ion intensities evolved during the NPF event in the bag reactor (Figure 2b-2f).

1. Cl , I , Cl_2 and ClI in gas phase: the intensities of I and Cl increased ca. 10 minutes before 14 nm particles appeared and decreased as the particles grew up (Figure 2b). Based on prior work of Burkholder et al. (2004); Jimenez et al. (2003); O'dowd et al. (2004), we suggested the photolysis of CH_2Cl_2 , $CHBrCl$, CH_3I and C_3H_7I was the source of halogen atoms (e.g., $CH_3I + h\nu \rightarrow CH_3 + I$), although we could not exclude the photolysis of other precursors like I_2 and HOI that are invisible to GC-MS and iodide-CIMS. There was a time lag of 20-25 minutes between the appearances of Cl and I and those of ClI and Cl_2 , which were probably resulted from anion exchange reactions of Cl^- and I^- with Cl atoms.

2. IO_2 , IO and $ClIO$ in gas phase: these species showed a similar time evolution to I and Cl atoms (Figure 2c). They could be from the reactions between I , ClI and O_3 (Saiz-Lopez et al., 2014). Sequential oxidation and aggregation reactions might have formed other halogen oxides (Gómez Mart ín et al., 2013), but they might not be detectable by iodide-CIMS.

3. INO_2 , $ClNO_2$ and INO_3 : INO_2 and $ClNO_2$ were detected in gas phase with similar time

evolution with halogen atoms and halogen oxides (Figure 2d). INO_3 was found in both gas and particle phases. INO_2 and INO_3 were usually thought to form upon the reactions $\text{I} + \text{NO}_2 + \text{M} \rightarrow \text{IONO} + \text{M}$ and $\text{IO} + \text{NO}_2 + \text{M} \rightarrow \text{IONO}_2 + \text{M}$ in the atmosphere (Saiz-Lopez et al., 2012), which seems to be unlikely in our bag reactor because NO_2 was not added. Considering NO_3^- was ubiquitous in the bag reactor of our experiment, it is likely that INO_2 and INO_3 formed via $\text{I}_2\text{O}_2 + \text{NO}_3^- \rightarrow \text{IO}_3^- + \text{IONO}$ and $\text{I}_2\text{O}_3 + \text{NO}_3^- \rightarrow \text{IO}_3^- + \text{IONO}_2$. These reaction pathways have been supported by theoretical calculation and flow tube mass spectrometry experiments (Gómez Mart í et al., 2022; Gómez Mart í et al., 2020). ClNO_2 was likely to form upon similar reaction between Cl_2O_2 and NO_3^- in the bag reactor.

3. HIO , HIO_2 and HIO_3 : HIO_3 seems to be the end product of above intermediates, because its gas-phase ion intensity kept on increasing during new particle growth (Figure 2e). Based on this fact, we assume that HIO_3 could be from $\text{I}_2\text{O}_5 + \text{H}_2\text{O} \rightarrow 2\text{HIO}_3$ or $\text{I}_2\text{O}_y + \text{NO}_3^- \rightarrow \text{IO}_3^- + \text{INO}_y$. On the other hand, HIO_3 was not detected in particle phase by iodide-CIMS, which is contrary to the offline analysis of quartz filter by HPLC-ICP-MS showing that total iodine was mostly dominated by IO_3^- peak. We speculate that HIO_3 might have been dehydrated to I_2O_5 under thermal desorption temperature up to 180°C in FIGAERO. The signals of IO^- , IO_2^- and HIONO_3^- (corresponding to HIO and HIO_2) were found in particle phase, but not in gas phase. He et al. (2021) proposed HIO_2 formation via $\text{I} + \text{H}_2\text{O} + \text{O}_3 \rightarrow \text{HIO}_2$ or $\text{I}_2\text{O}_2 + \text{H}_2\text{O} \rightarrow \text{HIO} + \text{HIO}_2$. With limit experimental evidence of our work, the exact formation pathways of HIO_x remains to be explored in future.

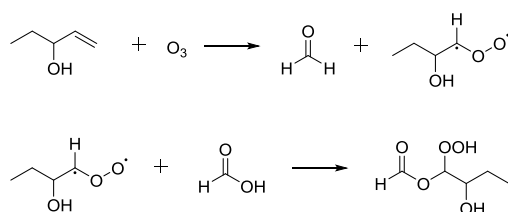
4. $\text{CH}_3\text{SO}_3\text{H}$, S_2^- , S_3^- , SO_3^- : We observed methane sulfonic acid ($\text{CH}_3\text{SO}_3\text{H}$, MSA) in both gas and particle phases. Gaseous MSA increased in the beginning, but decreased after new particles appeared (Figure 2f). Apparently, our measurement suggested MSA contributed to the growth of new particles, but it is unknown if it also participated in nucleation. We suggested S_2^- , S_3^- , SO_3^- ions observed in the particle phase were thermal decomposition products of MSA.

We noticed that CH_3I vapor was added as ion source reagent to the ion molecule reactor (IMR) of iodide-CIMS. It is likely that this extra CH_3I in the IMR might obscure the interpretation of the observed iodine containing clusters. We believed that ion source reagent CH_3I should have relatively small interference with inorganic iodine compounds from the bag reactor, on the basis of 2 facts: (1) ion source reagent CH_3I was added directly from permeation tube into the IMR. Without photolysis, ion source reagent CH_3I in the IMR should not become a source of I and I_xO_y . (2) the concentration of ion source reagent CH_3I and its potential products should be quite constant as long as O_3 was present in the IMR, which was not supported by the variable signals of I , ClI , IO_2 , IO , ClIO , HIO_3 ,

INO₂ and INO₃ in Figure 2.

3.2.2 Gaseous organic products

After ozone addition, a gradual transformation from C₁-C₃ precursors to C₅-C₈ gaseous products was observed during the NPF process (Figure 2h). In the meanwhile, the oxygen atom number of the compounds increased from 2-3 to 4-7 (Figure 2g). The formation of compounds with more carbon atoms than the parent VOCs is unlikely in the gas phase, except bimolecular reactions of stabilized Criegee intermediates (SCIs) that typically form upon alkene ozonolysis. Similar to isoprene ozonolysis (Riva et al., 2017; Inomata et al., 2014), we propose the SCI addition mechanism can also explain the transformation observed in our case: (1) C₄ SCIs formed upon the ozonolysis of CHO precursors with C=C double bonds (e.g., those observed by GC-MS in Table 1). (2) the insertion of C₄ SCIs into carboxylic acid precursors (e.g., those observed by CIMS in Table 1) produced oligomeric hydroperoxides. An example was shown in Scheme I for the reactions of most abundant ethyl vinyl carbinol (C₅H₁₀O), ozone and formic acid (CH₂O₂), but the same mechanism is also applicable for ethyl vinyl ketone (C₅H₈O) and other abundant C₂-C₅ carboxylic acids and hydroxyl carboxylic acids. As a result, a series of gaseous oligomeric hydroperoxides C₅H₁₀O₅, C₆H₁₀O₅, C₆H₁₂O₅, C₇H₁₂O₆, C₇H₁₄O₆, C₈H₁₄O₅, C₈H₁₆O₆, C₈H₁₆O₅ and C₉H₁₆O₆ were observed with high intensity by iodide-CIMS.



Scheme I

3.3 Particulate products

3.3.1 Relative mass contribution of organic carbon and iodine to new particles

In the dynamic mode experiments, O₃ in the bag reactor was kept at its maximum concentration 200 ppbv. With a prolonged residential time of 67 min, the particles grew to 102±23 nm, which was measured by the SMPS at the outlet of the bag reactor. The TOC and TI measurements show that organic compounds contributed more particle mass than iodine with TOC/(I+TOC) ratio of 96.1±2.9% (Table 2).

In the OH-enhanced experiment (dynamic mode), more particulate products were generated with enhanced oxidation capacity: TI in the particles increased by a factor of 10.8; TOC increased by a

factor of 2.7; particle number concentration increased by a factor of 7.4. On the other hand, particle size decreased to 73 nm and TOC/(TI+TOC) ratio decreased to 92.9% (Table 2). These differences indicate that more iodine nuclei were produced with enhanced oxidation capacity, probably via $\text{OIO} + \text{OH} \rightarrow \text{HOIO}_2$ (Plane et al., 2006) and $\text{O}(^3\text{P}) + \text{CH}_3\text{I} \rightarrow \text{IO} + \text{CH}_3$ (Teruel et al., 2004). Competitive uptake of condensing organic vapors onto these iodine nuclei limited the growth of individual new particles. Nevertheless, organic compounds overwhelmingly dominated over iodine in the mass contribution to new particle growth.

The significant organic contribution observed in the laboratory condition is generally consistent with TOC/(I+TOC) ratio of 98.2% in 10-56 nm new particles collected during a coastal I-NPF event in China (Yu et al., 2019), although TOC and TI during the field event are two orders of magnitude lower than those in the bag reactor (Table 2). Mean diameter of new particles was observed to be only 16 nm during the field event. But those small new particles are expected to grow into CCN active sizes, given longer residence time and uptake of more condensing vapors in the atmosphere (He et al., 2021).

3.3.2 Particulate organic products

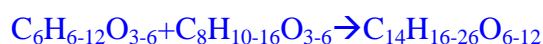
In the end of a typical ozonolysis experiment (dynamic mode), 100 and 364 new formulas were observed in the gas and particle phases, respectively, including 73 semi-VOCs appeared in both gas and particle phases. Those semi-VOCs accounted for 81 and 20% of total ion intensities of gaseous and particulate products, respectively. Being different from unimodal atom number distributions of gaseous products ($C_{\text{max}} = 7$ and $O_{\text{max}} = 5$, Figure 3b), particulate products were characterized by distinct bimodal or trimodal distribution of carbon number ($C_{\text{max}} = 8, 14$ and 16 , Figure 3c) and oxygen number ($O_{\text{max}} = 4$ and 8), implying possible dimer formation via accretion reactions in the particle phase.

ESI-Orbitrap MS differs from FIGAERO-iodide-CIMS in extraction method (ultrasonic solvent extraction from quartz fiber filter vs. thermal desorption from PTFE membrane filter), ionization source (electrospray ionization vs. iodide-adduct chemical ionization) and MS resolving power (70000 vs. 4500). The result showed that ESI-orbitrap MS and FIGAERO-iodide-CIMS detected 336 and 364 organic formulas, respectively, in the particle phase. 167 organic formulas were commonly observed by both methods, which accounted for 87% and 54% of total ion intensity of organic formulas by the two methods, respectively (Figure S1). As shown in Figure 3c and 3d, FIGAERO-iodide-CIMS had better sensitivity toward the organic compounds with more oxygen atoms (e.g., $O \geq 8$) and carbon atoms (e.g., $C \geq 10$). As a result, bimodal carbon and oxygen atom

number distributions were observed by FIGAERO-iodide-CIMS, but not ESI-orbitrap MS.

The measurement by ESI-orbitrap MS provided more insights about the formation mechanism of particulate products. We compared the 336 formulas detected by ESI-orbitrap MS in our study with the 414 formulas of isoprene ozonolysis SOA products (Nguyen et al., 2010) and 922 formulas of alpha-pinene ozonolysis SOA products (Putman et al., 2012) measured by the ESI-orbitrap MS. It was found that 72% of the formulas in this study can also be found in isoprene SOA, but only 39% can be found in alpha-pinene SOA. This seems to imply that some similar alkene ozonolysis reactions occurred in our system and isoprene ozonolysis.

For such a highly complex system full of various algae-emitted precursors, it is impossible to simply propose a reaction mechanism to explain the formation of all particulate products, nor to list all reactions occurring in the bag reactor. On the basis of particle-phase oligomer chemistry (Seinfeld and Pandis, 2016), especially the well-understood isoprene ozonolysis SOA chemistry (Nguyen et al., 2010; Inomata et al., 2014; Riva et al., 2017), we suggest a variety of accretion reactions without uniform oligomerization pattern (e.g., esterification, aldol condensation, hemiacetal reactions, peroxyhemiacetal formation and SCI reactions, etc.) transformed $O_{\max}=4$ and $C_{\max}=8$ multifunctional monomers (like alcohols, carbonyls, hydroperoxides, carboxylic acids) to $O_{\max}=8$ and $C_{\max}=14$ or 16 dimers. As an example, we used two simplified reaction equations to illustrate addition-type cross-oligomerization between C_6 and C_8 monomers and self-oligomerization of C_8 monomers, respectively:



in which the C_6 , C_8 , C_{14} and C_{16} formulas in the equations are among the most abundant ones observed in the particle phase by the iodide-CIMS.

4. Conclusions

Using a suite of mass spectrometers, we reported, for the first time, the chemical compositions of volatile precursors emitted by real-world coastal macroalgae and their gaseous and particulate oxidation products. In the presence of room light and ozone, the photolysis of halogenated $C_{1,3,5}$ alkanes ends up as HIO_3 and INO_3 . It was most likely HIO_3 initiated NPF and provided nuclei for the further condensation of other products like MSA and CHO compounds. Gas-phase SCI reactions and particle-phase accretion reactions transformed C_1 - C_6 and O_2 - O_3 precursors gradually to particulate products with $C_{\max}=8$, 14 and 16 and $O_{\max}=4$ and 8. As a result, organic carbon were found to

overwhelmingly dominated over iodine in the mass contribution to the new particle growth. Although our instruments did not allow the detection of nucleating clusters of iodine oxides or oxyacids, our study provided important complementary information to the ongoing laboratory and field researches of coastal I-NPF.

Data Availability

All data related to figures and tables in this study are archived and made available through Zenodo data repository <https://doi.org/10.5281/zenodo.6965859>.

Financial support.

This work was supported by the National Science Foundation of China (grant no. 41975831 and 42175131) and Start-up research funding from China University of Geosciences.

Competing Interests.

The authors declare that they have no conflict of interest.

Author contributions

HY designed the experiment. YW, XH and CX conducted the experiments. YW and HY analyzed the data and wrote the manuscript. QW and XG reviewed and revised the manuscript.

References

- Allan, J. D., Williams, P. I., Najera, J., Whitehead, J. D., Flynn, M. J., Taylor, J. W., Liu, D., Darbyshire, E., Carpenter, L. J., Chance, R., Andrews, S. J., Hackenberg, S. C., and McFiggans, G.: Iodine observed in new particle formation events in the Arctic atmosphere during ACCACIA, *Atmos. Chem. Phys.*, 15, 5599-5609, 10.5194/acp-15-5599-2015, 2015.
- Ashu-Ayem, E. R., Nitschke, U., Monahan, C., Chen, J., Darby, S. B., Smith, P. D., O'Dowd, C. D., Stengel, D. B., and Venables, D. S.: Coastal Iodine Emissions. 1. Release of I₂ by *Laminaria digitata* in Chamber Experiments, *Environmental Science & Technology*, 46, 10413-10421, 10.1021/es204534v, 2012.
- Baccarini, A., Karlsson, L., Dommen, J., Duplessis, P., Vüllers, J., Brooks, I. M., Saiz-Lopez, A., Salter, M., Tjernström, M., Baltensperger, U., Zieger, P., and Schmale, J.: Frequent new particle formation over the high Arctic pack ice by enhanced iodine emissions, *Nature Communications*, 11, 4924, 10.1038/s41467-020-18551-0, 2020.
- Beck, L. J., Sarnela, N., Junninen, H., Hoppe, C. J. M., Garmash, O., Bianchi, F., Riva, M., Rose, C., Peräkylä O., Wimmer, D., Kausiala, O., Jokinen, T., Ahonen, L., Mikkilä J., Hakala, J., He, X.-C., Kontkanen, J., Wolf, K. K. E., Cappelletti, D., Mazzola, M., Traversi, R., Petroselli, C., Viola, A. P., Vitale, V., Lange, R., Massling, A., Nøjgaard, J. K., Krejci, R., Karlsson, L., Zieger, P., Jang, S., Lee, K., Vakkari, V., Lampilahti, J., Thakur, R. C., Leino, K., Kangasluoma, J., Duplissy, E.-M., Siivola, E., Marbouti, M., Tham, Y. J., Saiz-Lopez, A., Petäjä T., Ehn, M., Worsnop, D. R., Skov, H., Kulmala, M., Kerminen, V.-M., and Sipilä M.: Differing Mechanisms of New Particle

345 Formation at Two Arctic Sites, *Geophysical Research Letters*, 48, e2020GL091334,
 346 <https://doi.org/10.1029/2020GL091334>, 2021.

347 Burkholder, J. B., Curtius, J., Ravishankara, A. R., and Lovejoy, E. R.: Laboratory studies of the
 348 homogeneous nucleation of iodine oxides, *Atmospheric Chemistry and Physics*, 4, 19-34,
 349 10.5194/acp-4-19-2004, 2004.

350 Donahue, N. M., Ortega, I. K., Chuang, W., Riipinen, I., Riccobono, F., Schobesberger, S., Dommen,
 351 J., Baltensperger, U., Kulmala, M., Worsnop, D. R., and Vehkamäki, H.: How do organic vapors
 352 contribute to new-particle formation?, *Faraday Discussions*, 165, 91-104, 10.1039/C3FD00046J,
 353 2013.

354 Ehn, M., Thornton, J. A., Kleist, E., Sipila, M., Junninen, H., Pullinen, I., Springer, M., Rubach, F.,
 355 Tillmann, R., Lee, B., Lopez-Hilfiker, F., Andres, S., Acir, I.-H., Rissanen, M., Jokinen, T.,
 356 Schobesberger, S., Kangasluoma, J., Kontkanen, J., Nieminen, T., Kurten, T., Nielsen, L. B.,
 357 Jorgensen, S., Kjaergaard, H. G., Canagaratna, M., Maso, M. D., Berndt, T., Petaja, T., Wahner, A.,
 358 Kerminen, V.-M., Kulmala, M., Worsnop, D. R., Wildt, J., and Mentel, T. F.: A large source of
 359 low-volatility secondary organic aerosol, *Nature*, 506, 476-479, 10.1038/nature13032, 2014.

360 Faxon, C., Hammes, J., Le Breton, M., Pathak, R. K., and Hallquist, M.: Characterization of organic
 361 nitrate constituents of secondary organic aerosol (SOA) from nitrate-radical-initiated oxidation of
 362 limonene using high-resolution chemical ionization mass spectrometry, *Atmospheric Chemistry
 363 and Physics*, 18, 5467-5481, 10.5194/acp-18-5467-2018, 2018.

364 Gómez Mart í, J. C., Lewis, T. R., James, A. D., Saiz-Lopez, A., and Plane, J. M. C.: Insights into
 365 the Chemistry of Iodine New Particle Formation: The Role of Iodine Oxides and the Source of
 366 Iodic Acid, *Journal of the American Chemical Society*, 144, 9240-9253, 10.1021/jacs.1c12957,
 367 2022.

368 Gómez Mart í, J. C., G ávez, O., Baeza-Romero, M. T., Ingham, T., Plane, J. M. C., and Blitz, M. A.:
 369 On the mechanism of iodine oxide particle formation, *Physical Chemistry Chemical Physics*, 15,
 370 15612-15622, 10.1039/c3cp51217g, 2013.

371 Gómez Mart í, J. C., Lewis, T. R., Blitz, M. A., Plane, J. M. C., Kumar, M., Francisco, J. S., and
 372 Saiz-Lopez, A.: A gas-to-particle conversion mechanism helps to explain atmospheric particle
 373 formation through clustering of iodine oxides, *Nature Communications*, 11, 4521,
 374 10.1038/s41467-020-18252-8, 2020.

375 He, X. C., Tham, Y. J., Dada, L., Wang, M., Finkenzeller, H., Stolzenburg, D., Iyer, S., Simon, M.,
 376 Kurten, A., Shen, J., Rorup, B., Rissanen, M., Schobesberger, S., Baalbaki, R., Wang, D. S.,
 377 Koenig, T. K., Jokinen, T., Sarnela, N., Beck, L. J., Almeida, J., Amanatidis, S., Amorim, A., Ataei,
 378 F., Baccarini, A., Bertozzi, B., Bianchi, F., Brilke, S., Caudillo, L., Chen, D., Chiu, R., Chu, B.,
 379 Dias, A., Ding, A., Dommen, J., Duplissy, J., El Haddad, I., Gonzalez Carracedo, L., Granzin, M.,
 380 Hansel, A., Heinritzi, M., Hofbauer, V., Junninen, H., Kangasluoma, J., Kemppainen, D., Kim, C.,
 381 Kong, W., Krechmer, J. E., Kvashin, A., Laitinen, T., Lamkaddam, H., Lee, C. P., Lehtipalo, K.,
 382 Leiminger, M., Li, Z., Makhmutov, V., Manninen, H. E., Marie, G., Marten, R., Mathot, S.,
 383 Mauldin, R. L., Mentler, B., Mohler, O., Muller, T., Nie, W., Onnela, A., Petaja, T., Pfeifer, J.,
 384 Philippov, M., Ranjithkumar, A., Saiz-Lopez, A., Salma, I., Scholz, W., Schuchmann, S., Schulze,
 385 B., Steiner, G., Stozhkov, Y., Tauber, C., Tome, A., Thakur, R. C., Vaisanen, O., Vazquez-Pufleau,
 386 M., Wagner, A. C., Wang, Y., Weber, S. K., Winkler, P. M., Wu, Y., Xiao, M., Yan, C., Ye, Q.,
 387 Ylisirnio, A., Zauner-Wieczorek, M., Zha, Q., Zhou, P., Flagan, R. C., Curtius, J., Baltensperger,
 388 U., Kulmala, M., Kerminen, V. M., Kurten, T., Donahue, N. M., Volkamer, R., Kirkby, J.,
 389 Worsnop, D. R., and Sipila, M.: Role of iodine oxoacids in atmospheric aerosol nucleation,
 390 *Science*, 371, 589-595, 10.1126/science.abe0298, 2021.

391 Heard, D. E., Read, K. A., Methven, J., Al-Haider, S., Bloss, W. J., Johnson, G. P., Pilling, M. J.,
 392 Seakins, P. W., Smith, S. C., Sommariva, R., Stanton, J. C., Still, T. J., Ingham, T., Brooks, B., De
 393 Leeuw, G., Jackson, A. V., McQuaid, J. B., Morgan, R., Smith, M. H., Carpenter, L. J., Carslaw,
 394 N., Hamilton, J., Hopkins, J. R., Lee, J. D., Lewis, A. C., Purvis, R. M., Wevill, D. J., Brough, N.,

395 Green, T., Mills, G., Penkett, S. A., Plane, J. M. C., Saiz-Lopez, A., Worton, D., Monks, P. S.,
 396 Fleming, Z., Rickard, A. R., Alfarra, M. R., Allan, J. D., Bower, K., Coe, H., Cubison, M., Flynn,
 397 M., McFiggans, G., Gallagher, M., Norton, E. G., O'Dowd, C. D., Shillito, J., Topping, D.,
 398 Vaughan, G., Williams, P., Bitter, M., Ball, S. M., Jones, R. L., Povey, I. M., O'Doherty, S.,
 399 Simmonds, P. G., Allen, A., Kinnersley, R. P., Beddows, D. C. S., Dall'Osto, M., Harrison, R. M.,
 400 Donovan, R. J., Heal, M. R., Jennings, S. G., Noone, C., and Spain, G.: The North Atlantic Marine
 401 Boundary Layer Experiment(NAMBLEX). Overview of the campaign held at Mace Head, Ireland,
 402 in summer 2002, *Atmos. Chem. Phys.*, 6, 2241-2272, 10.5194/acp-6-2241-2006, 2006.
 403 Huang, R.-J., Hoffmann, T., Ovadnevaite, J., Laaksonen, A., Kokkola, H., Xu, W., Xu, W., Ceburnis,
 404 D., Zhang, R., Seinfeld, J. H., and O'Dowd, C.: Heterogeneous iodine-organic chemistry
 405 fast-tracks marine new particle formation, *Proceedings of the National Academy of Sciences*, 119,
 406 e2201729119, 10.1073/pnas.2201729119, 2022.
 407 Inomata, S., Sato, K., Hirokawa, J., Sakamoto, Y., Tanimoto, H., Okumura, M., Tohno, S., and
 408 Imamura, T.: Analysis of secondary organic aerosols from ozonolysis of isoprene by proton
 409 transfer reaction mass spectrometry, *Atmospheric Environment*, 97, 397-405,
 410 <https://doi.org/10.1016/j.atmosenv.2014.03.045>, 2014.
 411 Jimenez, J. L., Bahreini, R., Cocker III, D. R., Zhuang, H., Varutbangkul, V., Flagan, R. C., Seinfeld,
 412 J. H., O'Dowd, C. D., and Hoffmann, T.: New particle formation from photooxidation of
 413 diiodomethane (CH₂I₂), *Journal of Geophysical Research: Atmospheres*, 108,
 414 <https://doi.org/10.1029/2002JD002452>, 2003.
 415 Kundu, S., Fisseha, R., Putman, A. L., Rahn, T. A., and Mazzoleni, L. R.: High molecular weight
 416 SOA formation during limonene ozonolysis: insights from ultrahigh-resolution FT-ICR mass
 417 spectrometry characterization, *Atmos. Chem. Phys.*, 12, 5523-5536, 10.5194/acp-12-5523-2012,
 418 2012.
 419 Kundu, S., Fisseha, R., Putman, A. L., Rahn, T. A., and Mazzoleni, L. R.: Molecular formula
 420 composition of β -caryophyllene ozonolysis SOA formed in humid and dry conditions,
 421 *Atmospheric Environment*, 154, 70-81, <https://doi.org/10.1016/j.atmosenv.2016.12.031>, 2017.
 422 Li, R., Palm, B. B., Ortega, A. M., Hlywiak, J., Hu, W., Peng, Z., Day, D. A., Knote, C., Brune, W. H.,
 423 de Gouw, J. A., and Jimenez, J. L.: Modeling the Radical Chemistry in an Oxidation Flow Reactor:
 424 Radical Formation and Recycling, Sensitivities, and the OH Exposure Estimation Equation, *The*
 425 *Journal of Physical Chemistry A*, 119, 4418-4432, 10.1021/jp509534k, 2015.
 426 Lopez-Hilfiker, F. D., Mohr, C., Ehn, M., Rubach, F., Kleist, E., Wildt, J., Mentel, T. F., Lutz, A.,
 427 Hallquist, M., Worsnop, D., and Thornton, J. A.: A novel method for online analysis of gas and
 428 particle composition: description and evaluation of a Filter Inlet for Gases and AEROSols
 429 (FIGAERO), *Atmospheric Measurement Techniques*, 7, 983-1001, 10.5194/amt-7-983-2014,
 430 2014.
 431 McFiggans, G., Coe, H., Burgess, R., Allan, J., Cubison, M., Alfarra, M. R., Saunders, R.,
 432 Saiz-Lopez, A., Plane, J. M. C., Wevill, D., Carpenter, L., Rickard, A. R., and Monks, P. S.: Direct
 433 evidence for coastal iodine particles from Laminaria macroalgae – linkage to emissions of
 434 molecular iodine, *Atmos. Chem. Phys.*, 4, 701-713, 10.5194/acp-4-701-2004, 2004.
 435 McFiggans, G., Bale, C. S. E., Ball, S. M., Beames, J. M., Bloss, W. J., Carpenter, L. J., Dorsey, J.,
 436 Dunk, R., Flynn, M. J., Furneaux, K. L., Gallagher, M. W., Heard, D. E., Hollingsworth, A. M.,
 437 Hornsby, K., Ingham, T., Jones, C. E., Jones, R. L., Kramer, L. J., Langridge, J. M., Leblanc, C.,
 438 LeCrane, J. P., Lee, J. D., Leigh, R. J., Longley, I., Mahajan, A. S., Monks, P. S., Oetjen, H.,
 439 Orr-Ewing, A. J., Plane, J. M. C., Potin, P., Shillings, A. J. L., Thomas, F., von Glasow, R., Wada,
 440 R., Whalley, L. K., and Whitehead, J. D.: Iodine-mediated coastal particle formation: an overview
 441 of the Reactive Halogens in the Marine Boundary Layer (RHAMBLe) Roscoff coastal study,
 442 *Atmospheric Chemistry and Physics*, 10, 2975-2999, 10.5194/acp-10-2975-2010, 2010.
 443 Monahan, C., Ashu-Ayem, E. R., Nitschke, U., Darby, S. B., Smith, P. D., Stengel, D. B., Venables,
 444 D. S., and O'Dowd, C. D.: Coastal Iodine Emissions: Part 2. Chamber Experiments of Particle

445 Formation from *Laminaria digitata*-Derived and Laboratory-Generated I₂, *Environmental Science*
446 & *Technology*, 46, 10422-10428, 10.1021/es3011805, 2012.

447 Nguyen, T. B., Bateman, A. P., Bones, D. L., Nizkorodov, S. A., Laskin, J., and Laskin, A.:
448 High-resolution mass spectrometry analysis of secondary organic aerosol generated by ozonolysis
449 of isoprene, *Atmospheric Environment*, 44, 1032-1042,
450 <https://doi.org/10.1016/j.atmosenv.2009.12.019>, 2010.

451 O'Dowd, C. D., Jimenez, J. L., Bahreini, R., Flagan, R. C., Seinfeld, J. H., Hämeri, K., Pirjola, L.,
452 Kulmala, M., Jennings, S. G., and Hoffmann, T.: Marine aerosol formation from biogenic iodine
453 emissions, *Nature*, 417, 632, 10.1038/nature00775, 2002.

454 O'Dowd, C. D., Facchini, M. C., Cavalli, F., Cebrunis, D., Mircea, M., Decesari, S., Fuzzi, S., Yoon,
455 Y. J., and Putard, J.-P.: Biogenically driven organic contribution to marine aerosol, *Nature*, 431,
456 676-680, 2004.

457 Plane, J. M. C., Joseph, D. M., Allan, B. J., Ashworth, S. H., and Francisco, J. S.: An Experimental
458 and Theoretical Study of the Reactions OIO + NO and OIO + OH, *The Journal of Physical*
459 *Chemistry A*, 110, 93-100, 10.1021/jp055364y, 2006.

460 Putman, A. L., Offenberg, J. H., Fisseha, R., Kundu, S., Rahn, T. A., and Mazzoleni, L. R.:
461 Ultrahigh-resolution FT-ICR mass spectrometry characterization of α -pinene ozonolysis SOA,
462 *Atmospheric Environment*, 46, 164-172, <https://doi.org/10.1016/j.atmosenv.2011.10.003>, 2012.

463 Riva, M., Budisulistiorini, S. H., Zhang, Z. F., Gold, A., Thornton, J. A., Turpin, B. J., and Surratt, J.
464 D.: Multiphase reactivity of gaseous hydroperoxide oligomers produced from isoprene ozonolysis
465 in the presence of acidified aerosols, *Atmospheric Environment*, 152, 314-322,
466 10.1016/j.atmosenv.2016.12.040, 2017.

467 Saiz-Lopez, A., Fernandez, R. P., Ordóñez, C., Kinnison, D. E., Gómez Mart í, J. C., Lamarque, J. F.,
468 and Tilmes, S.: Iodine chemistry in the troposphere and its effect on ozone, *Atmos. Chem. Phys.*,
469 14, 13119-13143, 10.5194/acp-14-13119-2014, 2014.

470 Saiz-Lopez, A., Plane, J. M. C., Baker, A. R., Carpenter, L. J., von Glasow, R., Gómez Mart í, J. C.,
471 McFiggans, G., and Saunders, R. W.: Atmospheric Chemistry of Iodine, *Chemical Reviews*, 112,
472 1773-1804, 10.1021/cr200029u, 2012.

473 Saunders, R. W. and Plane, J. M. C.: Formation Pathways and Composition of Iodine Oxide
474 Ultra-Fine Particles, *Environmental Chemistry*, 2, 299-303, <https://doi.org/10.1071/EN05079>,
475 2005.

476 Saunders, R. W., Kumar, R., Gómez Mart í, J. C., Mahajan, A. S., Murray, B. J., and Plane, J. M. C.:
477 Studies of the Formation and Growth of Aerosol from Molecular Iodine Precursor,
478 10.1524/zpch.2010.6143, 2010.

479 Seinfeld, J. H. and Pandis, S. N.: Atmospheric chemistry and physics: from air pollution to climate
480 change, 3rd, John Wiley and Sons. Inc., New York 2016.

481 Sellegri, K., Yoon, Y. J., Jennings, S. G., O'Dowd, C. D., Pirjola, L., Cautenet, S., Chen, H., and
482 Hoffmann, T.: Quantification of Coastal New Ultra-Fine Particles Formation from In situ and
483 Chamber Measurements during the BIOFLUX Campaign, *Environmental Chemistry*, 2, 260-270,
484 <https://doi.org/10.1071/EN05074>, 2005.

485 Sellegri, K., Pey, J., Rose, C., Culot, A., DeWitt, H. L., Mas, S., Schwier, A. N., Temime-Roussel, B.,
486 Charriere, B., Saiz-Lopez, A., Mahajan, A. S., Parin, D., Kukui, A., Sempere, R., D'Anna, B., and
487 Marchand, N.: Evidence of atmospheric nanoparticle formation from emissions of marine
488 microorganisms, *Geophysical Research Letters*, 43, 6596-6603,
489 <https://doi.org/10.1002/2016GL069389>, 2016.

490 Sipil ä M., Sarnela, N., Jokinen, T., Henschel, H., Junninen, H., Kontkanen, J., Richters, S.,
491 Kangasluoma, J., Franchin, A., Per äkyl ä O., Rissanen, M. P., Ehn, M., Vehkam äki, H., Kurten, T.,
492 Berndt, T., Pet ä ä T., Worsnop, D., Ceburnis, D., Kerminen, V.-M., Kulmala, M., and O'Dowd, C.:
493 Molecular-scale evidence of aerosol particle formation via sequential addition of HIO₃, *Nature*,
494 advance online publication, 10.1038/nature19314

495 <http://www.nature.com/nature/journal/vaop/ncurrent/abs/nature19314.html#supplementary-informati>
 496 [on](#), 2016.

497 Teruel, M. A., Dillon, T. J., Horowitz, A., and Crowley, J. N.: Reaction of O(3P) with the alkyl
 498 iodides: CF₃I, CH₃I, CH₂I₂, C₂H₅I, 1-C₃H₇I and 2-C₃H₇I, *Physical Chemistry Chemical*
 499 *Physics*, 6, 2172-2178, 10.1039/B316402K, 2004.

500 Vaattovaara, P., Huttunen, P. E., Yoon, Y. J., Joutsensaari, J., Lehtinen, K. E. J., O'Dowd, C. D., and
 501 Laaksonen, A.: The composition of nucleation and Aitken modes particles during coastal
 502 nucleation events: evidence for marine secondary organic contribution, *Atmos. Chem. Phys.*, 6,
 503 4601-4616, 10.5194/acp-6-4601-2006, 2006.

504 Wang, M., Zeng, L., Lu, S., Shao, M., Liu, X., Yu, X., Chen, W., Yuan, B., Zhang, Q., Hu, M., and
 505 Zhang, Z.: Development and validation of a cryogen-free automatic gas chromatograph system
 506 (GC-MS/FID) for online measurements of volatile organic compounds, *Analytical Methods*, 6,
 507 9424-9434, 10.1039/C4AY01855A, 2014.

508 Wang, M., Chen, D., Xiao, M., Ye, Q., Stolzenburg, D., Hofbauer, V., Ye, P., Vogel, A. L., Mauldin, R.
 509 L., 3rd, Amorim, A., Baccarini, A., Baumgartner, B., Brilke, S., Dada, L., Dias, A., Duplissy, J.,
 510 Finkenzeller, H., Garmash, O., He, X. C., Hoyle, C. R., Kim, C., Kvashnin, A., Lehtipalo, K.,
 511 Fischer, L., Molteni, U., Petäjä T., Pospisilova, V., Quéléver, L. L. J., Rissanen, M., Simon, M.,
 512 Tauber, C., Tomé A., Wagner, A. C., Weitz, L., Volkamer, R., Winkler, P. M., Kirkby, J., Worsnop,
 513 D. R., Kulmala, M., Baltensperger, U., Dommen, J., El-Haddad, I., and Donahue, N. M.:
 514 Photo-oxidation of Aromatic Hydrocarbons Produces Low-Volatility Organic Compounds,
 515 *Environmental science & technology*, 54, 7911-7921, 10.1021/acs.est.0c02100, 2020.

516 Wang, X., Hayeck, N., Brüggemann, M., Yao, L., Chen, H., Zhang, C., Emmelin, C., Chen, J.,
 517 George, C., and Wang, L.: Chemical Characteristics of Organic Aerosols in Shanghai: A Study by
 518 Ultrahigh-Performance Liquid Chromatography Coupled With Orbitrap Mass Spectrometry,
 519 *Journal of Geophysical Research: Atmospheres*, 122, 11,703-711,722,
 520 <https://doi.org/10.1002/2017JD026930>, 2017.

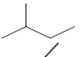
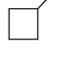
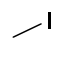
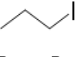
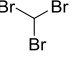
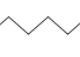
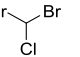
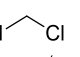

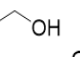
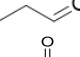
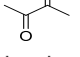
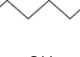
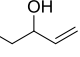
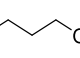
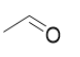
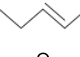
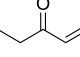
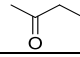
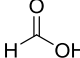
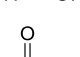
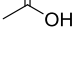
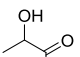
521 Whitehead, J. D., McFiggans, G. B., Gallagher, M. W., and Flynn, M. J.: Direct linkage between
 522 tidally driven coastal ozone deposition fluxes, particle emission fluxes, and subsequent CCN
 523 formation, *Geophysical Research Letters*, 36, doi:10.1029/2008GL035969, 2009.

524 Yan, C., Nie, W., Vogel, A. L., Dada, L., Lehtipalo, K., Stolzenburg, D., Wagner, R., Rissanen, M. P.,
 525 Xiao, M., Ahonen, L., Fischer, L., Rose, C., Bianchi, F., Gordon, H., Simon, M., Heinritzi, M.,
 526 Garmash, O., Roldin, P., Dias, A., Ye, P., Hofbauer, V., Amorim, A., Bauer, P. S., Bergen, A.,
 527 Bernhammer, A. K., Breitenlechner, M., Brilke, S., Buchholz, A., Mazon, S. B., Canagaratna, M.
 528 R., Chen, X., Ding, A., Dommen, J., Draper, D. C., Duplissy, J., Frege, C., Heyn, C., Guida, R.,
 529 Hakala, J., Heikkinen, L., Hoyle, C. R., Jokinen, T., Kangasluoma, J., Kirkby, J., Kontkanen, J.,
 530 Kürten, A., Lawler, M. J., Mai, H., Mathot, S., Mauldin, R. L., 3rd, Molteni, U., Nichman, L.,
 531 Nieminen, T., Nowak, J., Ojdanic, A., Onnela, A., Pajunoja, A., Petäjä T., Piel, F., Quéléver, L. L.
 532 J., Sarnela, N., Schallhart, S., Sengupta, K., Sipilä M., Tomé A., Tröstl, J., Väsänen, O., Wagner,
 533 A. C., Ylisirniö A., Zha, Q., Baltensperger, U., Carslaw, K. S., Curtius, J., Flagan, R. C., Hansel,
 534 A., Riipinen, I., Smith, J. N., Virtanen, A., Winkler, P. M., Donahue, N. M., Kerminen, V. M.,
 535 Kulmala, M., Ehn, M., and Worsnop, D. R.: Size-dependent influence of NO(x) on the growth
 536 rates of organic aerosol particles, *Science advances*, 6, eaay4945, 10.1126/sciadv.aay4945, 2020.

537 Yu, H., Ren, L., Huang, X., Xie, M., He, J., and Xiao, H.: Iodine speciation and size distribution in
 538 ambient aerosols at a coastal new particle formation hotspot in China, *Atmospheric Chemistry and*
 539 *Physics*, 19, 4025-4039, 10.5194/acp-19-4025-2019, 2019.

540

Table 1. Major volatile organic compounds emitted by macroalgae as potential NPF precursors, sorted by TIC peak area measured by GC/MS or MS peak intensity measured by iodide-CIMS

	Formula	Structure	Peak area/MS peak intensity
<i>GC/MS, non-CHO compounds</i>			
1	C ₅ H ₁₂		1.90×10 ⁶
2	C ₅ H ₁₀		1.59×10 ⁶
3	CH ₃ I		1.37×10 ⁶
4	C ₃ H ₇ I		7.60×10 ⁵
5	CHBr ₃		4.71×10 ⁵
6	C ₅ H ₁₁ I		3.75×10 ⁵
7	CHBr ₂ Cl		2.71×10 ⁵
8	CH ₂ Cl ₂		2.55×10 ⁵
9	C ₁₀ H ₁₆		2.26×10 ⁵
<i>GC/MS, CHO compounds</i>			
1	C ₂ H ₆ O		1.70×10 ⁷
2	C ₃ H ₆ O		1.38×10 ⁷
3	C ₄ H ₆ O ₂		1.30×10 ⁷
4	C ₆ H ₁₂ O		1.03×10 ⁷
5	C ₅ H ₁₀ O		1.00×10 ⁷
6	C ₄ H ₁₀ O		5.16×10 ⁷
8	C ₂ H ₄ O		3.46×10 ⁷
9	C ₆ H ₁₀ O		2.88×10 ⁷
7	C ₅ H ₈ O		1.45×10 ⁷
10	C ₄ H ₈ O		1.37×10 ⁷
<i>Iodide-CIMS</i>			
1	CH ₂ O ₂		1.58×10 ⁶
2	C ₂ H ₄ O ₂		9.52×10 ⁵
3	C ₃ H ₆ O ₃		9.21×10 ⁵
4	C ₆ H ₁₀ O ₃		4.44×10 ⁵

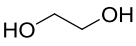
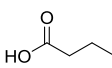
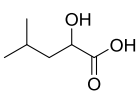
5	$\text{C}_2\text{H}_6\text{O}_2$		2.88×10^5
6	$\text{C}_4\text{H}_8\text{O}_2$		1.17×10^5
7	$\text{C}_6\text{H}_{12}\text{O}_3$		1.12×10^5

Table 2. Particle number concentration (N), mean diameter (D_p), total organic carbon (TOC) and total iodine (TI) of new particles with a residential time of 67 min in the bag reactor in the ozonolysis experiments and OH-enhanced experiment (dynamic mode). Those of 10-56 nm new particles collected by a nano Micro-Orifice Uniform Deposit Impactor (nano-MOUDI, MSP, Inc.) during an I-NPF event at a coastal site of Ningbo, China (Yu *et al.*, 2019) were also listed.

	TOC ($\mu\text{g m}^{-3}$)	TI ($\mu\text{g m}^{-3}$)	TOC/(TI+TOC)	N (cm^{-3})	D_p (nm)
ozonolysis experiments	45.6 \pm 9.7	0.88 \pm 0.34	96.1 \pm 2.9%	(5.58 \pm 2.04) $\times 10^4$	102 \pm 23
OH-enhanced experiment	125.3	9.5	92.9%	4.16 $\times 10^5$	73
I-NPF event at a coastal site of China	0.7	0.0135	98.2%	6.00 $\times 10^5$	16

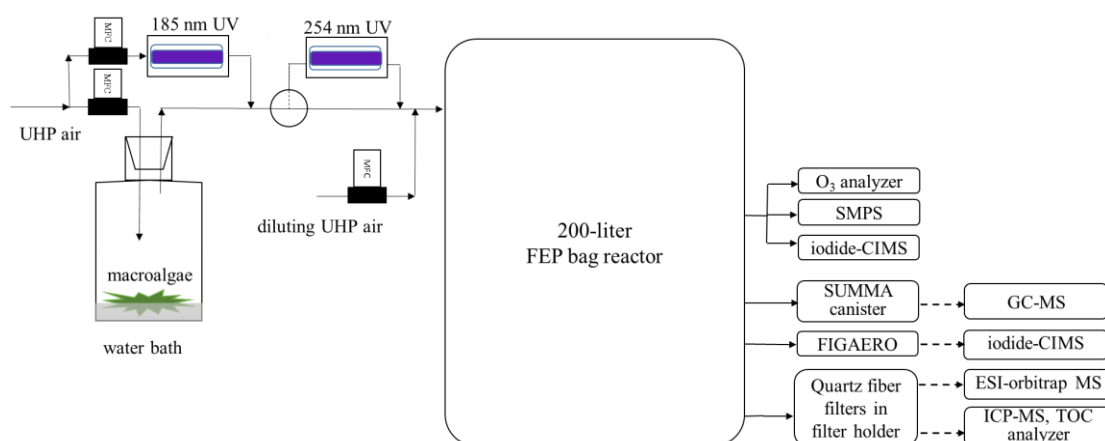


Figure 1. Schematic of experimental setup. Solid line: air flows. Dashed lines: sent for offline chemical analysis.

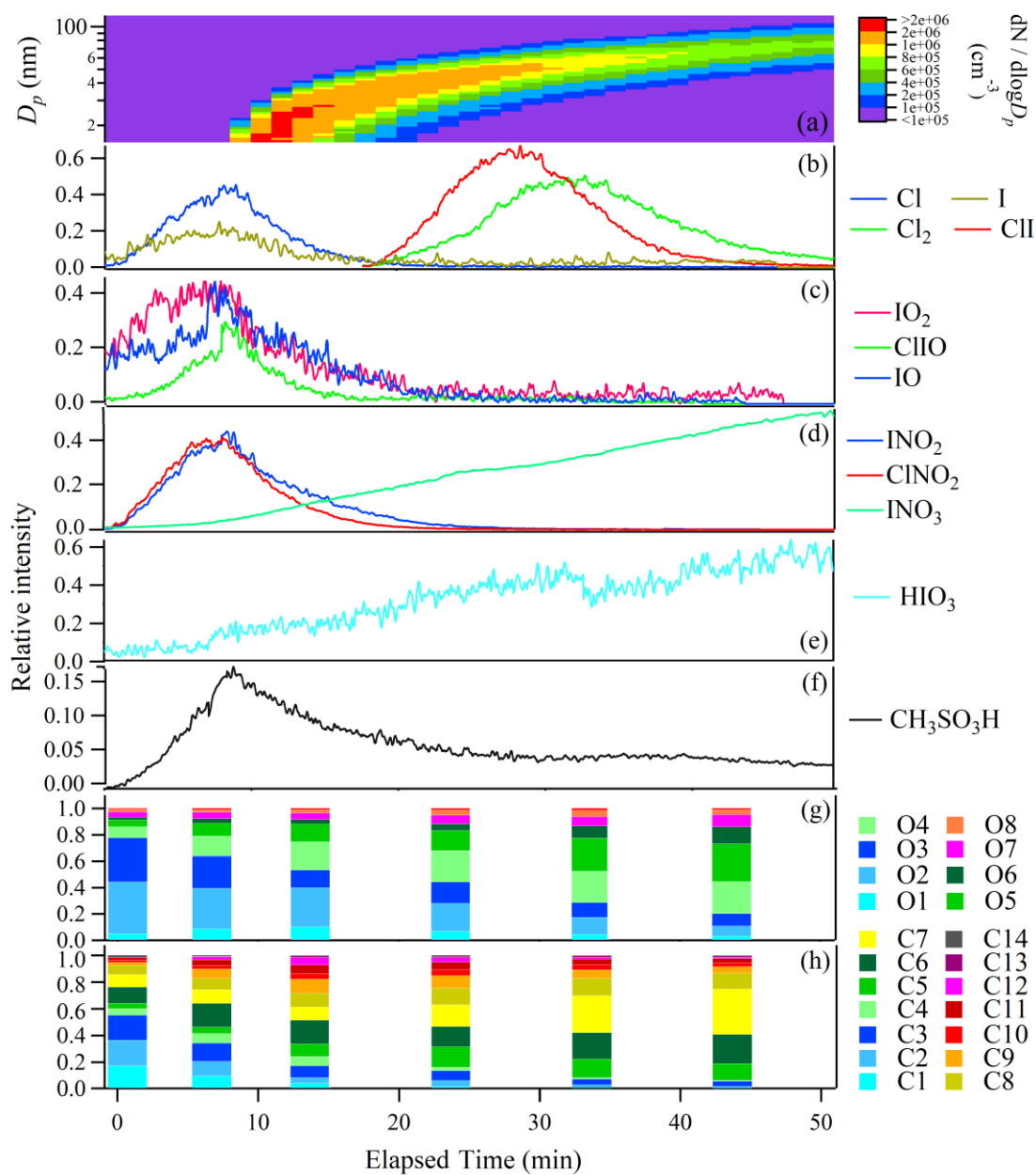


Figure 2. Time evolution of particle number size distribution (a) and relative intensities of gaseous molecules and radicals (b-f); the fractions of organic compounds grouped by O and C atom numbers in the selected time points (g-h) in a typical ozonolysis experiment (static mode). Time zero was set as the time when gaseous products first appeared.

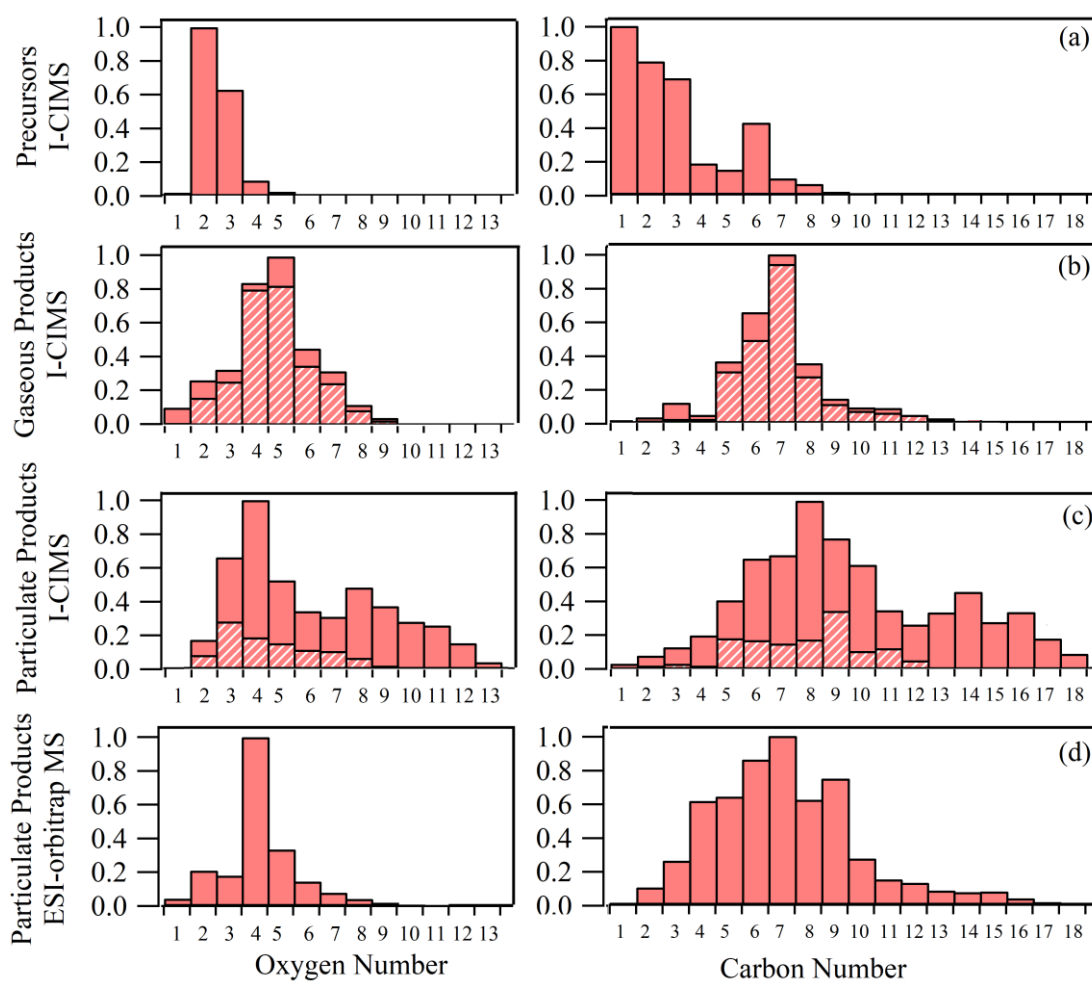


Figure 3. Oxygen and carbon atom number distributions of potential VOC precursors (a), gaseous products (b) and particulate products measured by iodide-CIMS (c), as well as the particulate products measured by ESI-orbitrap MS (d) in a typical ozonolysis experiment (dynamic mode). Hatched bars indicate the fractions of organic formulas observed in both gas and particle phases by iodide-CIMS.

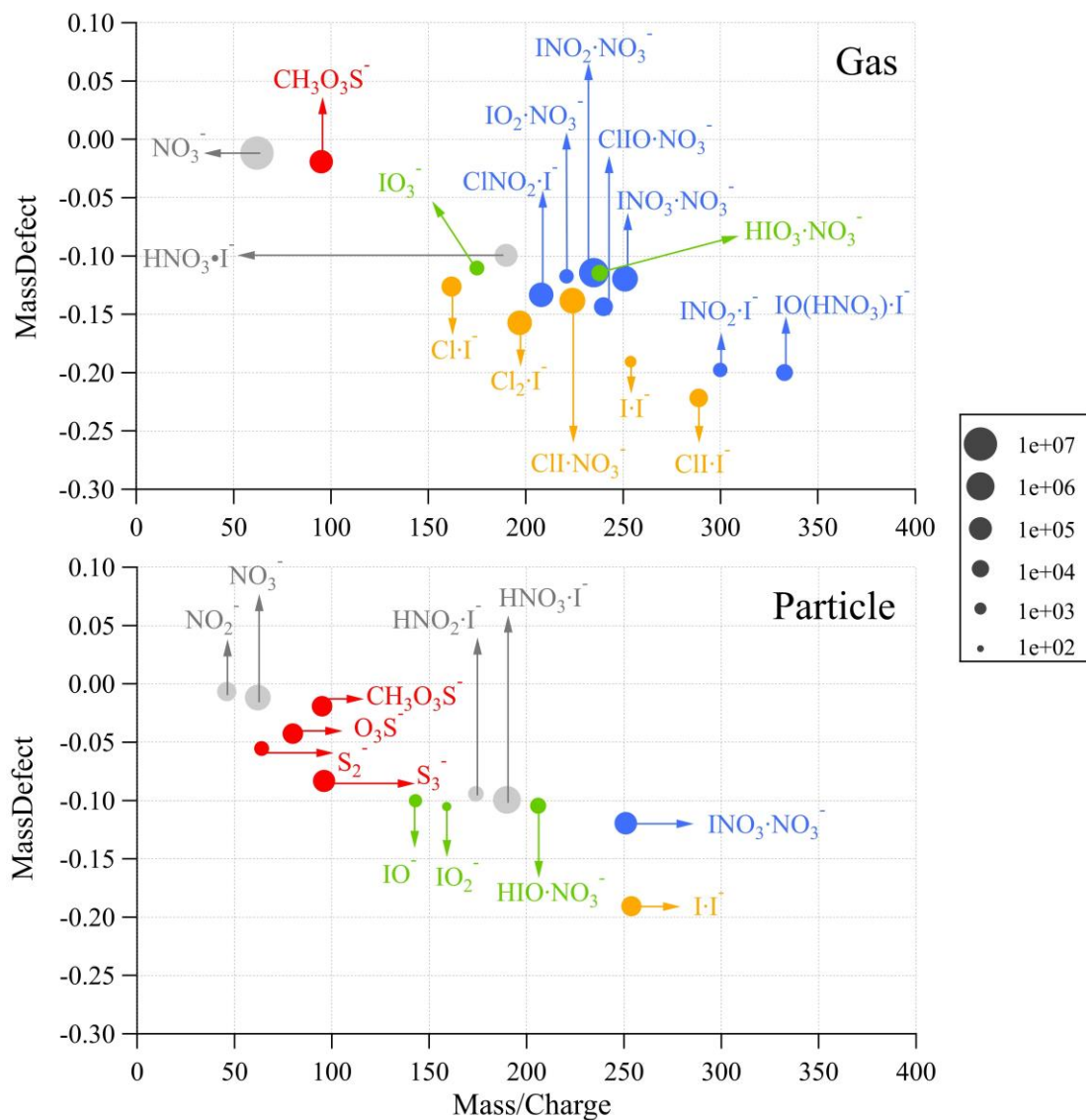


Figure 4. Integrated ion intensities of inorganic molecules and radicals in the gas phase (static mode) and particle phase (dynamic mode) measured by iodide-CIMS in a typical ozonolysis experiment. The ions were coded in color according to their elemental composition. For each ion cluster, parent neutral molecule is on the left hand side of middle dot, while the clustering ion I^- or NO_3^- is on the right hand side. Those without a clustering ion are shown as bare anions.